JACS
JOURNAL OF THE AMERICAN CHEMICAL SOCIETY

Article

pubs.acs.org/JACS

Nonracemic Antifolates Stereoselectively Recruit Alternate Cofactors and Overcome Resistance in *S. aureus*

Santosh Keshipeddy,[‡] Stephanie M. Reeve,[‡] Amy C. Anderson,* and Dennis L. Wright*

Department of Pharmaceutical Sciences, University of Connecticut, 69 North Eagleville Road, Storrs, Connecticut 06269, United States

Supporting Information

ABSTRACT: While antifolates such as Bactrim (trimethoprim-sulfamethoxazole; TMP-SMX) continue to play an important role in treating community-acquired methicillin-resistant *Staphylococcus aureus* (CA-MRSA), resistance-conferring mutations, specifically F98Y of dihydrofolate reductase (DHFR), have arisen and compromise continued use. In an attempt to extend the lifetime of this important class, we have developed a class of propargyl-linked antifolates (PLAs) that exhibit potent inhibition of the enzyme and bacterial strains. Probing the role of the configuration at the single propargylic stereocenter in these inhibitors required us to develop a new approach to nonracemic 3-aryl-1-butyne building blocks by the pairwise use of asymmetric conjugate addition and aldehyde dehydration protocols. Using this new route, a series of nonracemic PLA inhibitors was prepared and shown to possess potent enzyme inhibition (IC_{50} values <50 nM), antibacterial effects (several with MIC values <1 μg/mL) and to form stable ternary complexes with both wild-type and resistant mutants. Unexpectedly, crystal structures of a pair of individual enantiomers in the wild-type DHFR revealed that the single change in configuration of the stereocenter drove the selection of an alternative NADPH cofactor, with the minor α-anomer appearing with **R-27**. Remarkably, this cofactor switching becomes much more prevalent when the F98Y mutation is present. The observation of cofactor site plasticity leads to a postulate for the structural basis of TMP resistance in DHFR and also suggests design strategies that can be used to target these resistant enzymes.

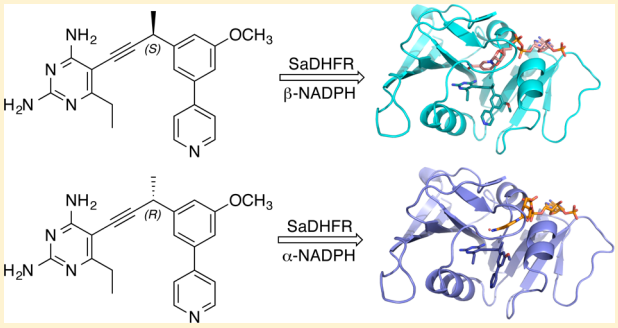

INTRODUCTION

Among the many classes of therapeutic agents, antibiotics differ in that their long-term utility is often compromised by the emergence of bacterial resistance, whereby previously efficacious agents lose their ability to effectively combat the current slate of pathogenic strains. Resistance can arise either through the acquisition of specific mechanisms (target mutation, efflux, or drug modifying enzymes) or the emergence of new strains that fall outside of a compound's traditional spectrum of coverage. However, medicinal chemistry efforts are often successful at overcoming these resistance mechanisms through rational modification of the antibiotic structure, leading to successive generations of agents with improved activity. Often, these efforts require innovations in synthetic chemistry to efficiently access significant new derivatives.

Perhaps one of the most common organisms that displays extensive resistance profiles is *Staphylococcus aureus*, specifically the methicillin-resistant strains of *S. aureus* (MRSA). In community-acquired strains of MRSA, trimethoprim-sulfamethoxazole (TMP-SMX, Bactrim) is first-line therapy, targeting the essential enzymes dihydrofolate reductase (DHFR) and dihydropteroate synthase (DHPS), respectively.[1,2] However, resistance to Bactrim now accounts for a significant proportion of the circulating strains.[3−6] The F98Y point mutation in DHFR is the pivotal mutation clinically observed to confer high levels of resistance to trimethoprim,[5] primarily resulting in a change in entropy of ligand binding and a loss of synergy or binding cooperativity between trimethoprim and the NADPH cofactor.[7] Interestingly, the binding cooperativity between cofactor and the DHF substrate is not significant compared to TMP.[8] New generations of antifolates that effectively target the mutated forms of DHFR will be critical for prolonging the utility of this class of antibiotics.

We have been focused on the development of next-generation antifolates that can target both the wild-type and predominant TMP-resistant strains. Using a structure-based approach, we have developed an advanced lead series of inhibitors that displays low nanomolar inhibition of the wild-type DHFR and potent activity against a range of MRSA strains (MIC values 0.04−0.72 μg/mL) and other important Gram-positive pathogens.[9−12] This compound class is characterized by a unique propargylic linker between the polar diaminopyrimidine headgroup and a hydrophobic biaryl domain as exemplified in Figure 1. Alkyne functionality is unique and structurally distinct from other unsaturated units in that the

Received: February 13, 2015
Published: June 22, 2015

DOI: 10.1021/jacs.5b01442
J. Am. Chem. Soc. 2015, 137, 8983−8990

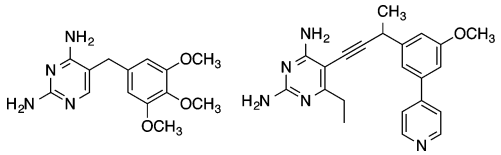

Figure 1. Trimethoprim (TMP) and a potent PLA.

linear, cylindrical nature of the group allows it to fit through very narrow passages in a binding site such as in the case of ponatinib binding the mutant form of Bcr-Abl.[13,14] Our work has shown that this group is important for achieving an optimal fit to the active site and in conferring potency against TMP-resistant species of DHFR;[15] furthermore, it is both chemically and metabolically stable.[16]

Our prior studies with racemic mixtures of propargyl-linked antifolates (PLAs) show that this class of compounds maintains good inhibitory activity against F98Y mutants of *S. aureus* DHFR.[10] Structural studies with a series of PLAs showed that the branched substituents from the propargylic position are proximal to the cofactor binding site and may provide compensatory interactions with NADPH as well as providing conformational control of the biaryl ring system in both wild-type and mutant enzymes. Therefore, investigating the role of the stereogenicity of the propargyl center in governing activity against the mutant enzymes became a priority. These molecules possess a challenging stereogenic center containing both acetylenic and aryl substituents; this is an uncommon arrangement with very limited synthetic access. Herein, we describe an efficient asymmetric route to these compounds that was used to prepare a variety of enantiopure PLAs. Excitingly, many of these compounds are the most potent inhibitors to date of both the wild-type and F98Y forms of *S. aureus* DHFR. Interestingly, individual crystal structures of the *S. aureus* DHFR enzyme bound to members of an enantiomeric pair show that the stereogenic center drives not only the conformation of the biaryl system and interactions with the enzyme, but also drives the placement of the cofactor, NADPH, revealing plasticity in the cofactor binding site. The detailed investigation of the bound structure, inhibition profile and antibacterial activity of the pairs of enantiomers presented here allowed us to refine a model of antifolate resistance in DHFR that postulates a role for plasticity in the cofactor site, enhanced by the predominant mutant binding an alternative cofactor that greatly attenuates inhibitor potency.

EXPERIMENTAL METHODS

Evaluation of Antibacterial Activity. Minimum inhibitory concentrations were determined according to Clinical and Laboratory Standards Institute guideline's standard microdilution broth assay using a final inoculum of 5×10^5 CFU/mL in Isosensitest Broth (Oxoid). MICs were determined using *S. aureus* quality control strain 43300 (ATCC) and a lab generated F98Y mutant strain.[10] The MIC was defined as the lowest concentration of inhibitor to visually inhibit growth. Growth was monitored at A_{600} after 18 h of incubation at 37 °C. MICs were colorimetrically confirmed using Presto Blue (Life Technologies).

Enzyme Expression and Purification. Procedures for cloning the Sa(WT)DHFR construct in pET41a(+) have been previously reported.[10] The recombinant Sa (WT) enzyme was overexpressed in *E. coli* BL21 (DE3) (Invitrogen) cells and purified using nickel affinity chromatography (5Prime). Protein was desalted using a PD-10 column (GE Healthcare) into buffer containing 20 mM Tris pH 7.0, 20% glycerol, 0.1 mM EDTA, and 2 mM DTT. Aliquots were stored at −80 °C.

Enzymatic Inhibition Assays. IC_{50} values were determined by enzyme inhibition assays, which were performed in triplicate by monitoring the rate of NADPH oxidation by DHFR via absorbance at 340 nm. The reaction was performed at room temperature in buffer containing 20 mM TES, 50 mM KCl, 0.5 mM EDTA, 10 mM β-mercaptoethanol, and 1 mg/mL BSA using 0.1 mM NADPH and 2 μg/mL enzyme. One microliter of inhibitor at 0.001−1 μM in DMSO was added to enzyme/NADPH mixture and allowed to incubate for 5 min before the addition of 0.1 mM DHF in 50 mM TES, pH 7.0. The mixtures had a final DMSO concentration of 1.8%.

Minimum Inhibitory Concentrations with Efflux Inhibitors. Minimum inhibitory concentrations were determined as described previously, containing either (+)-verapamil[17] (Sigma-Aldrich, stored at 20 mg/mL in water) at 100 μg/mL, reserpine[17] (Sigma-Aldrich, stored at 4 mg/mL in DMSO) at 20 μg/mL or thioridazine[12] (Sigma-Aldrich, stored at 20 mg/mL in DMSO) at 12.5 μg/mL, final DMSO concentrations of solutions at 0.05%, 0.11% and 0.6%, respectively Inhibitor stocks kept at 20 mg/mL in DMSO, compounds tested at 10 μg/mL. The MIC was defined as the lowest concentration of inhibitor to visually inhibit growth. Growth was monitored at A_{600} after 18 h of incubation at 37 °C. MIC values were colorimetrically confirmed using Presto Blue (Life Technologies).

Minimum Inhibitory Concentrations with Thymidine. Minimum inhibitory concentrations were determined in Isosensitest Broth (Oxoid) containing thymidine (Sigma-Aldrich) at 10 μg/mL. The MIC was defined as the lowest concentration of inhibitor to visually inhibit growth. Growth was monitored at A_{600} after 18 h of incubation at 37 °C. MICs were colorimetrically confirmed using Presto Blue (Life Technologies).

On-Site Dissociation Experiments. The steady-state NADPH turnover rate was determined by performing enzyme inhibition assays following 18 h of 4 °C incubation with 2 μg/mL purified DHFR, 100 μM NADPH, and 50 μM inhibitor in buffer containing 20 mM TES, 50 mM KCl, 0.5 mM EDTA, 10 mM β-mercaptoethanol, and 1 mg/mL BSA. The reaction was initiated with 0.1 mM DHF and monitored at an absorbance of 340 nm. The steady-state NADPH rate was extrapolated from data by converting the slope of A_{340} vs time to change in NADPH concentration using a molar extinction coefficient of 6.2×10^3 L mol^{-1}cm^{-1}.

Crystal Structure Determination. Sa(WT)DHFR was cocrystallized with NADPH and **R-27** and **S-27** using the hanging drop vaporization method. Purified protein (17 and 21 mg/mL, respectively) was incubated with 2 mM NADPH (Sigma-Aldrich) and 1 mM inhibitor in DMSO for 2h on ice. Equal volumes of the protein/cofactor solutions were mixed with an optimized crystallization solution containing 13% PEG 10 000, 0.1 M sodium acetate, 0.1 M MES pH 6.0−6.25, and 0.5% γ-butyrolactone. When stored at 4 °C, conditions typically yielded crystals within 7 days. Crystals were frozen in cryo-protectant buffer containing 25% glycerol. High-resolution data were collected on the X25A Beamline at Brookhaven National Laboratories for Sa(WT)DHFR/NADPH/**R-27** and at the Rigaku HighFlux HomeLab Protein Crystallography X-ray system at the University of Connecticut for Sa(WT)/NADPH/**S-27**.

Data for Sa(WT)DHFR/NADPH/**R-27** and **S-27** were indexed and scaled using HKL2000 or d*TREK, respectively. Phaser was used to identify molecular replacement solutions for the structures of both structures using PDB/3F0Q as a probe.[11] The programs Coot and Phenix were used for structure refinement until acceptable R_{work} and R_{free} were achieved.[18,19] Structural geometry was evaluated via Procheck[20] and Ramachandran plots.

RESULTS AND DISCUSSION

Traditionally, acetylenic moieties have been far less frequently employed in pharmaceutical products than alkyl or alkenyl linkers but in recent years have increased in prevalence.[21,22] One of the main drivers of this increase is advances in preparative methodology that allow for the mild introduction of acetylenic units into complex molecules, most notably those relying on palladium-mediated coupling reactions. However,

DOI: 10.1021/jacs.5b01442
J. Am. Chem. Soc. 2015, 137, 8983−8990

methods for the preparation of complex alkynes, specifically nonracemic versions, have been less thoroughly developed and limits access to diverse alkyne building blocks. In earlier inhibitor generations, we had established the asymmetric propargylic center through an Evan's asymmetric alkylation.[23] Subsequently, Fu disclosed an elegant asymmetric catalytic aryl propargylation approach to these inhibitors.[24] However, the presence of basic heterocycles in the third-generation inhibitors proved problematic and the earlier routes were plagued both by ready epimerization when the center was adjacent to electron-withdrawing functionality and by facile isomerization to the conjugated allene. Herein, we report a versatile route to these nonracemic 3-aryl-1-butynes that should prove generally valuable in the synthesis of sensitive pharmaceutical compounds.

It was envisioned that the application of an asymmetric conjugate addition strategy to suitably deactivated styrene derivative **5** could be a good solution to this problem, provided that a relatively straightforward conversion of the acceptor functionality in **4** to a terminal alkyne **3** without allene formation would be possible. This route insulates the benzylic stereocenter from the necessary electron-withdrawing carbonyl functionality and thus significantly decreases the potential for racemization (Scheme 1).

Scheme 1. Retrosynthetic Analysis of Non-Racemic Propargyl-Linked Antifolates

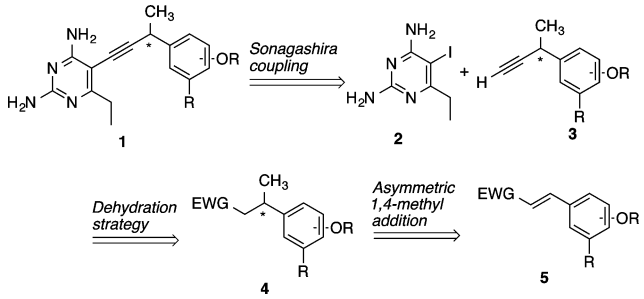

While there have been several reports on effective asymmetric conjugate addition reactions of carbon nucleophiles to electron poor olefins, the addition of methyl onto cinnamates has remained particularly challenging, and many systems deliver the methyl addition products in poor yields or with low enantioselectivity.[25−28] Feringa and co-workers[29,30] recently evaluated copper-catalyzed methyl additions to cinnamate thioesters in the presence of chiral phosphine ligands. The Feringa study suggested that application to the PLA building blocks would be limited, as the presence of required alkoxy groups on the cinnamate aryl ring was shown to dramatically decrease the reactivity of the cinnamate, leading to poor reaction yields. However, we were intrigued by their observation that an electron-withdrawing chlorine atom was beneficial and speculated that delaying installation of the C-ring until after the methyl addition would permit the precursor bromine to balance the electron donating methoxy groups and permit an efficient addition to take place. Initial studies showed that the presence of the deactivating bromide on the cinnamate provided compensatory electronic effects, leading to better yields of the product relative to the nonbrominated congeners. Further improvement to the reaction was made by an elevation in temperature to −55 °C and an increase in catalyst loading. Utilizing these optimized conditions, it was possible to secure good isolated yields and excellent enantioselectivities of the addition products even with two electron-donating alkoxy groups present on the aromatic ring (see **13** and **15** in Table 1).

Through this process, we were able to prepare five enantiomeric pairs (**11−15 R/S**) with differential electron donating substitution on the aromatic moiety. The subsequent cross-coupling reaction to the aryl bromide presented some concern owing to the known propensity of thioesters to engage directly in palladium-catalyzed processes. Pleasingly, palladium-promoted Suzuki reaction between the thio-cinnamates (**11−15 R/S**) and heteroaryl boronic acid proceeded exclusively at the bromide to deliver the biaryl derivatives in very good yields (Scheme 2).

With an optimized conjugate addition/Suzuki coupling protocol in place, the second key process in the route was the conversion of thiocarbonyl group to the corresponding terminal acetylene without racemization of the single stereocenter or isomerization to the allene. This transformation was accomplished smoothly in two steps by initial conversion to the aldehyde (**16−20 R/S**) through catalytic hydrogenation followed by application of an underutilized direct aldehyde

Table 1. Asymmetric Conjugate Addition of Methyl Group onto Cinnamic Acid Thioesters

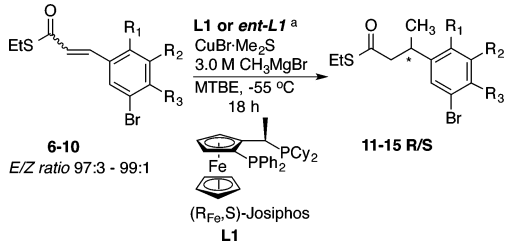

product entry	R_1	R_2	R_3	% yield[b] with **L1**	ee[c] with **L1**	% yield[b] with ***ent*-L1**	ee[c] with ***ent*-L1**
11	OMe	H	H	75	95[d] (S)[e]	77	92 (R)[e]
12	H	OMe	H	84	93 (S)	80	93 (R)
13	H	OMe	OMe	72	97 (S)	71	95 (R)
14	H	H	OMe	52	90 (S)	55	94 (R)
15	H	OCH_2	OCH_2	80	90 (S)	82	94[d] (R)

[a]Conditions: **6−10** (1 equiv), MeMgBr (3.3 equiv), $CuBr{\cdot}SMe_2$ (9 mol %), **L1 or ent-L1** (10 mol %) in MTBE at −55 °C, 18 h. [b]Isolated yield. [c]Determined by chiral HPLC. [d]ee also determined after asymmetric conjugate addition reaction. For entries **11−15** ee was determined after the formation of alkynes **21−25**. [e]Absolute configuration assigned based on Feringa's work and crystal structures presented here.

DOI: 10.1021/jacs.5b01442
J. Am. Chem. Soc. 2015, 137, 8983−8990

Scheme 2. Synthesis of Non-Racemic Propargyl-Linked Antifolates

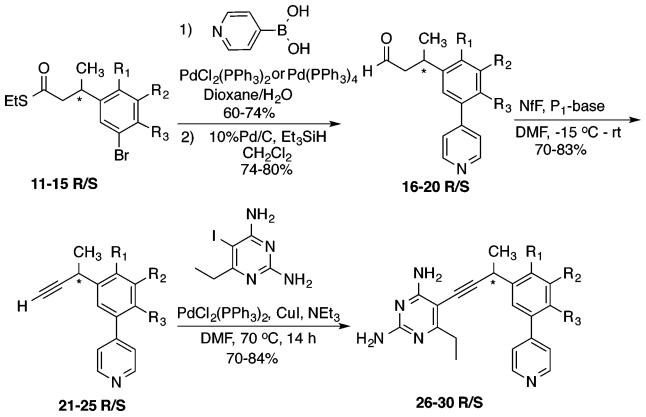

dehydration reaction.[31] Exposure of our highly functionalized aldehydes to nonaflyl fluoride and a strong phosphazane base resulted in a smooth conversion to the terminal alkynes (**21**–**25 R/S**) with only trace amounts of allene being observed. Importantly, determination of the enantiomeric excess for the derivatives revealed that no epimerization of the propargylic methyl group had taken place under the strongly basic conditions of the reactions. Final Sonogashira coupling of these alkynes with 6-ethyl-5-iodo-2,4-diaminopyrimidine as previously described,[23] delivered the enantiomerically pure inhibitor series for biological study (Scheme 2). Importantly, it was also possible to effectively scale-up these routes to gram-scale level and allowed the direct preparation of 900 mg of inhibitor **S-26** for ongoing in vivo studies.

Structural Studies. Crystal structures of SaDHFR/NADPH/**R-27** and SaDHFR/NADPH/**S-27** reveal unexpected and significant differences in the binding mode of the two enantiomers with the enzyme. After collection of diffraction data (2.69 and 2.16 Å, respectively; figures showing electron density are found in SI Table S1 and Figures S1 and S2), the structures were determined by molecular replacement with probe molecule PDB ID 3F0Q.[32] Both crystals belong to space group $P6_122$ and possess equivalent crystal contacts, none of which are near the active sites. The structure of Sa/NADPH/**S-27** reported here is identical to the previously reported structure of *S. aureus* DHFR/NADPH/rac-**27**, suggesting that the ternary complex with **S-27** is the more thermodynamically stable complex relative to that formed with **R-27**. In the structure of Sa/NADPH/**S-27**, the enzyme binds the extended, β-form of NADPH and there are a number of key van der Waals contacts between the inhibitor and the nicotinamide ring of the cofactor involving each of the four carbons of the unique propargyl linker that characterizes this compound series. In addition to the expected interactions between the diaminopyrimidine and residues Asp 27, Val 31, and Leu 28 there are contacts between Leu 28, Ile 50, Met 42, and Leu 54 and the hydrophobic 4-arylpyridine moiety that favor a coplanar arrangement between the two joined aromatic rings. The acetylenic linker is critical for penetrating the narrow space near Phe92 (Figure 2a).

Surprisingly, the structure of Sa/NADPH/**R-27** reveals a major change at the NADPH cofactor binding site, whereby the nicotinamide and ribose rings are displaced (~3.2 Å) relative to the standard β-form of NADPH and the displaced carboxamide forms three water-mediated hydrogen bonds to the protein

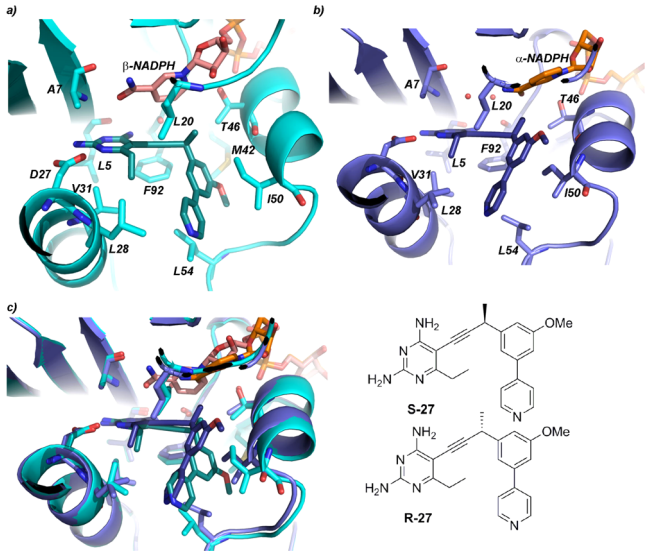

Figure 2. Crystal structures of wild-type *S. aureus* DHFR bound to cofactor and inhibitors: (a) compound **S-27** (teal) and β-NADPH (salmon) or (b) compound **R-27** (purple) and α-NADPH (orange). Panel c shows a superposition of the two structures.

rather than directly contacting Ala 7 (Figure 2b). Despite this displacement, the pyrophosphate tail and adenine nucleotide are ultimately placed in the identical binding sites. We had first observed this altered binding mode for NADPH in structures of mutant (F98Y) SaDHFR bound to earlier generation propargyl-linked antifolates.[10] In fact, the structure of an earlier generation PLA (UCP115A; PDB ID 3FQF) in complex with the wild-type enzyme binds β-NADPH with 100% occupancy but shows an exclusive preference for the displaced form of NADPH with the F98Y mutant enzyme. In general, there is attenuated Sa(F98Y) enzyme inhibition with increasing occupancy of the displaced NADPH observed in the crystal structure.[10] Overlaying the wild-type Sa/NADPH/**R-27** structure reported here with PDB ID:3FQF reveals complete superposition, including two of the key water molecules bridging the carboxamide (see SI Figure S3). These changes in NADPH were initially attributed to a change in conformation of β-NADPH; however, further analysis has revealed that the conformational change is actually a consequence of a change in configuration at the anomeric carbon of the ribose ring to produce the α-form. Although NADPH is known to exist in an equilibrium between the two anomers, with a distribution of approximately 1.5% α-form,[33] it is rarely observed in crystal structures with any NADPH-dependent reductase. Furthermore, while β-NADPH is the common cofactor used in DHFR catalysis, α-NADPH can be an effective reducing agent for the structurally distinct R67 DHFR[34] and has recently been shown to be a natural substrate for renalase, which catalyzes both an anomerization and oxidation reaction to regenerate β-$NADP^+$.[33]

Here, wild-type Sa/NADPH/**R-27** binds α-NADPH at 100% occupancy, where α-NADPH is primarily stabilized by a projection of the methyl group of the R-enantiomer into a pocket formed by Phe 92 and Thr 46. In this position, Asn 18 forms a hydrogen bond with the ribose hydroxyl from α-NADPH. Overall, the cofactor change to α-NADPH diminishes the interactions between the inhibitor and the cofactor. Specifically, only the propargylic carbon forms a van der Waals interaction with α-NADPH, whereas all four carbon

DOI: 10.1021/jacs.5b01442
J. Am. Chem. Soc. 2015, 137, 8983–8990

Table 2. Biological Activity of the Propargyl-Linked Antifolates

inhibitor[a]	R_1	R_2	R_3	Sa IC_{50}[c] (nM)	Sa IC_{50}[d] (nM)	Sa(F98Y) IC_{50}[c] (nM)	NADPH rate (μM/min)	NADPH rate F98Y (μM/min)	MICwild-type *S. aureus* (μg/mL)	MICSa(F98Y) (μg/mL)
R-26	OMe	H	H	19 ± 1	464 ± 27	3503 ± 100	−4.571	−10.129	1.25	10
S-26	OMe	H	H	11 ± 0.7	37 ± 5	261 ± 16	−0.454	−1.514	0.078	1.25
R-27	H	OMe	H	15 ± 0.7	69 ± 5	510 ± 50	−0.919	−4.959	0.3125	5
S-27	H	OMe	H	18 ± 2	155 ± 5	111 ± 6	−0.965	−0.975	0.0391	0.625
R-28	H	OMe	OMe	46 ± 4	26 ± 3	267 ± 3	−0.850	ND[e]	1.25	5
S-28	H	OMe	OMe	74 ± 6	98 ± 8	2048 ± 91	−2.712	ND[e]	2.5	20
R-29	H	H	OMe	202 ± 20	458 ± 37	12,714 ± 700	−19.944	−9.588	1.25	40
S-29	H	H	OMe	35 ± 6	211 ± 12	2030 ± 60	−0.428	−2.701	0.3125	20
R-30	H	OCH_2	OCH_2	46 ± 6	78 ± 4	1179 ± 19	−1.241	−6.515	0.3125	2.5
S-30	H	OCH_2	OCH_2	35 ± 2	45 ± 6	176 ± 14	−0.359	−1.45	0.078	1.25
TMP				23 ± 3	77 ± 4	1700 ± 19	−0.505	−6.178	0.3125	10

[a]

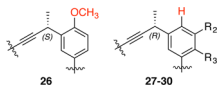

Note the change in the descriptor assignment (i.e., *S*) for the inhibitor **26** because of the 2′-OMe substitution. [b]Dissociation experiments were performed in duplicate and MIC, IC50 experiments were performed in triplicate. Average NADPH rates for no-inhibitor controls were −138.3 μM/min for Sa DHFR and −103.53 μM/min for Sa F98Y DHFR. [c]Measured with 5 min preincubation of enzyme and inhibitor. [d]Measured with no preincubation of enzyme and inhibitor. [e]ND: not determined.

atoms in the linker form interactions with β-NADPH. Independent of the NADPH switch, Ile 50 undergoes a second significant conformational change in order to accommodate a change in enantiomeric preference. Both a 1.5 Å displacement of the protein backbone and a change in the side chain rotamer of Ile 50 are necessary to accommodate the R-configuration of **27**. Therefore, when a racemic mixture of the ligand is present, the protein would need to undergo a significant conformational change to bind the opposite enantiomer.

Biological Studies. Evaluation of the ten enantiopure inhibitors revealed that all of the compounds maintain strong inhibition of the wild type bacterial dihydrofolate reductase with the majority of inhibitors having IC_{50} values less than 50 nM (Table 2). The compounds also display significant antibacterial activity against a strain of MRSA (ATCC 43300), with the most active congeners showing an 8-fold increase in activity relative to trimethoprim. In contrast to TMP, the PLAs were designed to form alternative and additional contacts with residues in the active site produced by the stereoselective steering of the biaryl domain by the branching at the propargylic position and to become less dependent on the cofactor for binding cooperativity toward the enzyme (Figure 2). Accordingly, inhibitors such as **S-26**, **S-27**, and **S-30** are much more potent against the F98Y mutant enzyme than TMP. The PLAs exhibit a loss in activity of only 3.3−12-fold as compared to TMP that loses 74-fold against the mutant enzyme. The PLAs also retain very good antibacterial activity (MIC values 0.625−1.25 μg/mL).

As antibacterial activity is also highly dependent on the degree and persistence of the blockade of the essential targeted pathway, we investigated the target inhibition profile of the enantiomers with DHFR. Previous studies have shown the importance of conformational changes in the catalytic cycle of DHFR,[35,36] including the presence of two isoforms of the apo enzyme. Ligands may possess modulated affinity to the isoforms, but eventually stabilize a single conformation of the enzyme.[35] By comparing enzyme inhibition values using the standard incubation of enzyme and inhibitor (5 min) with those that did not have a preincubation step, we attempted to detect differences in the capacity of enantiomers to quickly form a stable, inhibited ternary complex. The results show an increase in the observed IC_{50} value with the magnitude of increase depending on the specific pairs. For example, the dioxalane derivatives, **R/S-30**, display only marginal increases in IC_{50} value while the 2′-methoxy derivative, **R-26**, shows a more substantial increase in observed IC_{50} (24.4-fold) as well as a more significant difference between the two enantiomers (3.4- vs 24.4-fold). Overall, these experiments suggest that some inhibitors require the preincubation step in order to form a high affinity complex; a conformational change in the enzyme may be occurring during this incubation.

Dissociation of the complex was determined for five pairs of enantiomers. Dissociation rates were determined by following experiments outlined for neuraminidase,[37] whereby various inhibitors were incubated with the enzyme for a period of time followed by the addition of substrate and measurement of the reaction. Here, each inhibitor was incubated with DHFR and NADPH for an 18-h period to form the ternary complex. After the incubation period, dihydrofolate was added to the complex and catalysis, measured by the formation of the oxidized cofactor, was monitored over a 1-h time period. With the exception of **R/S-27**, for which the rates were similar, these studies show that there is a differential rate of dissolution of the inhibited complex depending on the enantiomer present (Table 2 and SI Figure S4).

Overall, the target inhibition profile experiments show that several inhibitors, including **S-26**, **R-28**, **S-28**, **R-30**, and **S-30**, appear to form an inhibited complex immediately upon mixing. Furthermore, several inhibitors, including **S-26**, **R-27**, **S-27**, **R-28**, **S-29**, and **S-30** have a relatively slow rate of dissolution of that ternary complex. As effective antibacterial agents must quickly form an effective and long-lasting inhibitory target complex, these results are promising, especially for compounds **S-26** and **S-30** that possess both of these qualities.

We then employed dissociation experiments in order to evaluate the dissolution of the ternary complexes with

DOI: 10.1021/jacs.5b01442
J. Am. Chem. Soc. 2015, 137, 8983−8990

Sa(F98Y) DHFR, NADPH and inhibitor. We found that the complex composed of Sa(F98Y)DHFR/NADPH/TMP was the least stable of all complexes evaluated compared to its wild-type counterpart (Table 2 and SI Figure S5) with a dissolution rate of −6.18 μM/min, 12.4-fold greater than the complex of wild-type enzyme and TMP. Interestingly, when the complexes between Sa(F98Y) and the enantiomers were evaluated, many are quite stable. For example, **S-26**, **S-27**, **S-29**, and **S-30** have very similar rates of dissolution with the mutant enzyme relative to those with the wild-type enzyme.

Interestingly, there is a noticeable difference in the antibacterial activity between the two antipodes in most of the derivatives. For example, while the S-enantiomer of **26** shows a modest 1.7-fold increase in enzyme inhibitory potency relative to the R-stereoisomer, the antibacterial activity of the S-isomer is 16-fold greater. This same trend is also seen in compound **30**.

Bacterial membrane permeability, selective efflux, possible second target activity, and differences in target inhibition profile are some of the most likely determinants of the differential antibacterial activity. Although differences between enantiomers with regard to bacterial membrane permeability cannot be completely ruled out, this is less likely as the major descriptors of permeability such as partition coefficient, molecular weight, or topological polar surface area are identical for both enantiomers. Moreover, the inherent flexibility about the single stereogenic center limits overall differences in the shape of the molecules. In order to evaluate the role of efflux transporters, we measured antibacterial activity in the presence of reserpine, verapamil and thioridazine, three known efflux pump inhibitors that have been shown to inhibit the activity of the majority of pumps in *S. aureus*, including NorA, MepA, and SepA.[38,39] A decrease in the MIC value of at least 8-fold in the presence of the pump inhibitors is accepted as evidence of significant efflux transport activity. As MIC values in the presence of these efflux pump inhibitors do not change significantly (SI Table S2), it is unlikely that the different antibiotic potencies of the enantiomers are related to selective efflux. Next, we examined the potential that the enantiomers have differential affinity to a possible second target in the bacteria that would lead to increased antibacterial activity. As the PLAs are inhibitors of the folic acid biosynthetic pathway that is primarily responsible for the production of deoxythymidine monophosphate, rescue experiments were conducted to measure MIC values in the presence of the end-product, thymidine. With 10 μg/mL thymidine, MIC values rose to 5−10 μg/mL (see SI Table S3), indicating on-target activity. As the pairs of enantiomers possess the same MIC values in the presence of thymidine, it is unlikely that the enantiomers have differential affinity for a second target outside the pyrimidine biosynthesis pathway. Notably, however, these experiments do not necessarily determine whether the compounds coinhibit thymidylate synthase or enzymes upstream of DHFR since the end-product thymidine captures multiple enzymes on the pathway. Overall, there are many factors that play significant roles in determining antibacterial activity. While we have attempted to investigate the roles of a few important variables here, we recognize the complexity of the bacteria and stipulate that a number of forces may be at play to determine the differential activity between the enantiomers.

SUMMARY

In this study, the pairwise use of asymmetric conjugate addition reactions and a direct aldehyde dehydration process was pivotal for the preparation of several enantiomeric pairs of propargyl-linked antifolates. Biological studies show that the configuration of this chiral center provides essential conformational control of the biaryl moiety as well as projects functionality specifically proximal to the cofactor. These interactions are critical to maintaining potency against the enzyme with the F98Y point mutation as well as providing superior potency against the wild-type enzyme. Accordingly, several of the compounds demonstrated significant levels of activity against both the wild-type MRSA and mutants harboring the key F98Y mutation. A noteworthy observation is that two enantiomers, containing only a single stereogenic center, drove a unique change in the adjacent NADPH binding site, leading to the binding of a minor component of the natural cofactor. Remarkably, these molecules produce an identical structural effect as the key clinical F98Y mutation, thus proving invaluable in refining our understanding of the structural basis of a resistance mutation on the plasticity of the cofactor binding site. The molecules also reveal a strategy for overcoming the primary mechanism for antifolate resistance in MRSA.

As observed in the two crystal structures reported here, the wild-type enzyme possesses greater plasticity in the cofactor binding site than may be initially anticipated, permitting the binding of the minor anomer of the cofactor. It is not known whether α-NADPH actively reduces dihydrofolate. Previous experiments show that it is not active using *E. coli* DHFR or DHFR from L1210 cells;[34] however, it is active with R67 DHFR,[34] glutathione reductase[40] and old yellow enzyme.[41] This plasticity in the cofactor binding site is reminiscent of the structures with the F98Y mutation where the mutation is responsible for altering the population distribution of the β-NADPH-bound complexes. There is a conserved organized water network observed in the wild-type enzyme that becomes substantially more energetically favorable upon introduction of the tyrosine mutation, whereby the phenolic hydroxyl group interacts strongly with this network. Upon binding of β-NADPH to either wild-type or the F98Y mutant, this network is displaced. In the background of the F98Y mutation, complexes with simply the water network (apo enzyme) or, as observed with the PLAs, the water network engaged with α-NADPH, are likely to be more prevalent than in the wild-type enzyme (see Figure 3 for a representative cartoon).

Interestingly, the crystal structure of TMP bound to Sa(F98Y) shows bound β-NADPH and almost completely superimposes with the structure of the wild-type enzyme bound to TMP and β-NADPH, making it difficult to explain the 74-fold loss in enzyme inhibition. However, while this structure of Sa(F98Y)/β-NADPH/TMP may be thermodynamically stable in the crystal, there is significant evidence that the formation of the intermediate binary complexes are less readily formed. Isothermal calorimetry experiments reveal attenuated binding for both TMP and β-NADPH in the formation of binary complexes;[7] additionally, dissociation experiments shown here reveal a very fast dissolution of the complex between Sa(F98Y) and TMP. Although studies on the catalytic cycle of DHFR have described a classical binding order where NADPH binds prior to DHF,[35] various solution experiments[7,8] have shown that the binding of TMP and NADPH can occur in any order, ultimately leading to a stable ternary complex. Additionally,

DOI: 10.1021/jacs.5b01442
J. Am. Chem. Soc. 2015, 137, 8983−8990

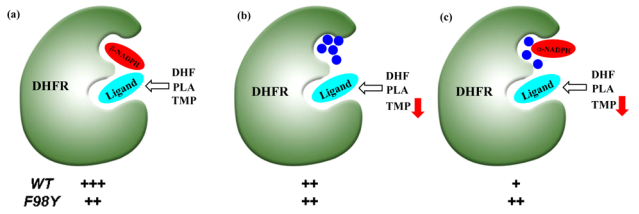

Figure 3. Proposed Mechanism of F98Y-Mediated Resistance. DHFR can exist in multiple states, bound to the major (a) and minor (c) anomers of NADPH as well as the solvated form (b). As the binary complex with β-NADPH (a) is believed to predominate in the wild-type enzyme, TMP, or the PLAs can bind, form a stable complex, and exert a strong antibiotic effect. However, the F98Y mutation alters the distribution between these three states, leading to an increase in (b) and/or (c) at the expense of (a), effectively protecting a portion of the enzyme from forming a stable ternary complex with TMP and allowing bacterial growth. The binding modes of the PLA chemotype allow these inhibitors to evade this mechanism of resistance by effectively competing with DHF in all three states, as PLA inhibitors bind regardless of the cofactor status.

several structures of binary complexes of DHFR indicate that mimics of DHF and various inhibitors can bind the apo enzyme.[42−45] While TMP can bind the enzyme without β-NADPH, it is only when β-NADPH binds that a stable ternary complex is formed.[8] As dihydrofolate does not bind cooperatively with cofactor,[8] it likely forms complexes with either anomer or the apo enzyme, eventually undergoing catalysis when productive complexes with β-NADPH arise. Therefore, TMP resistance is mediated by an increase in Sa(F98Y) species lacking bound β-NADPH and hence, lowering affinity for TMP, yet reserving a pool of enzyme capable of binding and ultimately reducing dihydrofolate. As we show here that the PLAs can bind to complexes with both α-NADPH and β-NADPH, it is expected that they could form inhibitory complexes irrespective of the cofactor. As PLAs do not appear to depend on the presence of β-NADPH for binding, it is anticipated that they will also bind effectively to the apo enzyme. The combination of these possible binding events leads to a more effective blockade of the folate pathway in both wild-type and F98Y enzymes. The ability of PLAs to form ternary complexes with α-NADPH raises the intriguing possibility that the enzyme is simultaneously bound to two inhibitory molecules and that sequential replacement of both would be required before catalytic activity could be restored.

In conclusion, we have demonstrated the importance of pursuing enantiomerically pure PLAs as the configuration drives major structural, biochemical, and antibacterial effects and aids in the translation to studies in vivo. We have confirmed that this center is critical for activity and that the preferred configuration is a parameter that is dependent on the overall composition of the inhibitor. Analysis of ten enantiomerically pure PLAs identified an exemplary inhibitor, **S-27**, which is potent at both the enzymatic and cellular levels against wild-type and mutant F98Y DHFR. The efficiency of the synthetic strategy described herein allows us to prepare compound for ongoing in vivo efficacy analysis. Interestingly, the crystal structures of one pair of enantiomers reveal that the least active enantiomer complex bound an alternative cofactor, α-NADPH. Concurrently, it was observed that the least active enantiomer of the pair biochemically mirrors the effect of the F98Y mutation in DHFR that leads to trimethoprim resistance. These observations lead to a refined model of the mechanism of resistance in which F98Y hinders cofactor binding and obstructs the formation of the ternary complex required for stability. Further analysis indicates that the PLAs evade this mechanism by effectively binding and disabling both the wild-type and mutant enzymes. The alteration of the cofactor binding site by a key active site mutation represents a highly unusual mechanism for drug resistance.

■ ASSOCIATED CONTENT

Supporting Information

Crystallographic data collection and refinement statistics, experimental procedures, spectral data, and biological data are provided. The crystallographic coordinates are deposited in the Protein Data Bank (PDB codes 4XEC and 4TU5). The Supporting Information is available free of charge on the ACS Publications website at DOI: 10.1021/jacs.5b01442.

■ AUTHOR INFORMATION

Corresponding Authors

*amy.anderson@uconn.edu
*dennis.wright@uconn.edu

Author Contributions

‡These authors contributed equally.

Notes

The authors declare no competing financial interest.

■ ACKNOWLEDGMENTS

We gratefully acknowledge grant support from the NIH (R01AI111957) to D.L.W. and A.C.A. Data for this study were measured at beamline X25 of the National Synchrotron Light Source with the help of Dr. Annie Heroux. We also thank Pablo Gainza and Bruce Donald for discussion of α-NADPH.

■ REFERENCES

(1) Frei, C.; Miller, M.; Lewis, J.; Lawson, K.; Hunter, J.; Oramasionwu, C.; Talbert, R. *J. Am. Board Fam. Med.* **2010**, *23*, 714.
(2) Nathwani, D.; Morgan, M.; Masterton, R.; Dryden, M.; Cookson, B.; French, G.; Lewis, D. *J. Antimicrob. Chemother.* **2008**, *61*, 976.
(3) Klevens, M.; Edwards, J.; Tenover, F.; McDonald, L. C.; Horan, T.; Gaynes, R. *NNISS Clin. Infect. Dis.* **2006**, *42*, 389.
(4) Wisplinghoff, H.; Bischoff, T.; Tallent, S.; Seifert, H.; Wenzel, R.; Edmond, M. *Clin. Infect. Dis.* **2004**, *39*, 309.
(5) Dale, G.; Broger, C.; D'Arcy, A.; Hartman, P.; DeHoogt, R.; Jolidon, S.; Kompis, I.; Labhardt, A.; Langen, H.; Locher, H.; Page, M.; Stuber, D.; Then, R.; Wipf, B.; Oefner, C. *J. Mol. Biol.* **1997**, *266*, 23.
(6) Houvinen, P.; Sundstrom, L.; Swedberg, G.; Skold, O. *Antimicrob. Agents Chemother.* **1995**, *39*, 279.
(7) Heaslet, H.; Harris, M.; Fahnoe, K.; Sarver, R.; Putz, H.; Chang, J.; Subramanyam, C.; Barreiro, G.; Miller, J. R. *Proteins* **2009**, *76*, 706.
(8) Feeney, J.; Birdsall, B.; Kovalevskaya, N. V.; Smurnyy, Y. D.; Navarro Peran, E. M.; Polshakov, V. I. *Biochemistry* **2011**, *50*, 3609.
(9) Viswanathan, K.; Frey, K.; Scocchera, E.; Martin, B.; Swain, P.; Alverson, J.; Priestley, N.; Anderson, A.; Wright, D. *PLoS One* **2012**, *7*, e29434.
(10) Frey, K.; Liu, J.; Lombardo, M.; Bolstad, D.; Wright, D.; Anderson, A. *J. Mol. Biol.* **2009**, *387*, 1298.
(11) Frey, K.; Lombardo, M.; Wright, D.; Anderson, A. *J. Struc. Biol.* **2010**, *170*, 93.
(12) Frey, K.; Viswanathan, K.; Wright, D.; Anderson, A. *Antimicrob. Agents Chemother.* **2012**, *56*, 3556.
(13) Huang, W.-S.; Metcalf, C. A.; Sundaramoorthi, R.; Wang, Y.; Zou, D.; Thomas, R. M.; Zhu, X.; Cai, L.; Wen, D.; Liu, S.; Romero, J.; Qi, J.; Chen, I.; Banda, G.; Lentini, S. P.; Das, S.; Xu, Q.; Keats, J.; Wang, F.; Wardwell, S.; Ning, Y.; Snodgrass, J. T.; Broudy, M. I.; Russian, K.; Zhou, T.; Commodore, L.; Narasimhan, N. I.;

DOI: 10.1021/jacs.5b01442
J. Am. Chem. Soc. 2015, 137, 8983−8990

Mohemmad, Q. K.; Iuliucci, J.; Rivera, V. M.; Dalgarno, D. C.; Sawyer, T. K.; Clackson, T.; Shakespeare, W. C. *J. Med. Chem.* **2012**, *53*, 4701.
(14) O'Hare, T.; Shakespeare, W. C.; Zhu, X.; Eide, C.; Rivera, V. M.; Wang, F.; Adrian, L.; Zhou, T.; Huang, W.-S.; Xu, Q.; Metcalf, C. A.; Tyner, J.; Loriaux, M.; Corbin, A.; Wardwell, S.; Ning, Y.; Keats, J.; Wang, Y.; Sundaramoorthi, R.; Thomas, R. M.; Zhou, D.; Snodgrass, J. T.; Commodore, L.; Sawyer, T. K.; Dalgarno, D. C.; Deininger, M.; Druker, B.; Clackson, T. *Cancer Cell* **2009**, *16*, 401.
(15) Zhou, W.; Scocchera, E.; Wright, D.; Anderson, A. *Med. Chem. Comm.* **2013**, *4*, 908.
(16) Zhou, W.; Viswanathan, K.; Hill, D.; Anderson, A.; Wright, D. *Drug Metab. Distrib.* **2012**, *40*, 2002.
(17) Aeschlimann, J. R.; Dresser, L. D.; Kaatz, G. W.; Rybak, M. J. *Antimicrob. Agents Chemother.* **1999**, *43*, 335.
(18) Adams, P.; Afonine, P.; Bunkóczi, G.; Chen, V.; Davis, I.; Echools, N.; Headd, J.; Hung, L.-W.; Kapral, G.; Grosse-Kunstleve, R.; McCoy, A.; Moriarty, N.; Oeffner, R.; Read, R.; Richardson, D.; Richardson, J.; Terwilliger, T.; Zwart, P. *Acta Crystallogr.* **2010**, *D66*, 213.
(19) Emsley, P.; Cowtan, K. *Acta Crystallogr.* **2004**, *D60*, 2126.
(20) Laskowski, R.; MacArthur, M.; Moss, D.; Thornton, J. *J. Appl. Crystallogr.* **1993**, *26*, 283.
(21) King, A.; Yasuda, N. *Top. Organomet. Chem.* **2004**, *6*, 205.
(22) Chinchilla, R.; Najera, C. *Chem. Rev.* **2014**, *114*, 1783.
(23) Bolstad, D.; Bolstad, E.; Frey, K.; Wright, D.; Anderson, A. *J. Med. Chem.* **2008**, *51*, 6839.
(24) Smith, S.; Fu, G. *J. Am. Chem. Soc.* **2008**, *130*, 12645.
(25) Lopez, F.; Harutyunyan, S. R.; Meetsma, A.; Minnaard, A. J.; Feringa, B. L. *Angew. Chem., Int. Ed.* **2005**, *44*, 2752.
(26) Palais, L.; Babel, L.; Quintard, A.; Belot, S.; Alexakis, A. *Org. Lett.* **2010**, *12*, 1988.
(27) Wang, S.; Loh, T. *Chem. Commun.* **2010**, *46*, 8694.
(28) Wang, S. Y.; Lum, T. K.; Ji, S. J.; Loh, T. P. *Adv. Synth. Catal.* **2008**, *350*, 673.
(29) Des Mazery, R.; Pullez, M.; Lopez, F.; Harutyunyan, S. R.; Minnaard, A. J.; Feringa, B. L. *J. Am. Chem. Soc.* **2005**, *127*, 9966.
(30) Ruiz, B. M.; Geurts, K.; Fernandez-Ibanez, M. Å.; Horst, B. T.; Minnaard, A. J.; Feringa, B. L. *Org. Lett.* **2007**, *9*, 5123.
(31) Lyapkalo, I. M.; Vogel, M. A. K.; Boltukhina, E. V.; Vavrik, J. *Synlett.* **2009**, 558.
(32) Frey, K.; Georgiev, I.; Donald, B.; Anderson, A. *Proc. Natl. Acad. Sci., U. S. A.* **2010**, *107*, 13707.
(33) Beaupre, B.; Carmichael, B.; Hoag, M.; Shah, D.; Moran, G. *J. Am. Chem. Soc.* **2013**, *135*, 13980.
(34) Smith, S.; Burchall, J. *Proc. Natl. Acad. Sci., U. S. A.* **1983**, *80*, 4619.
(35) Schnell, J. R.; Dyson, H. J.; Wright, P. E. *Annu. Rev. Biophys. Biomol. Struct.* **2004**, *33*, 119.
(36) Boehr, D. D.; McElheny, D.; Dyson, H. J.; Wright, P. E. *Science* **2006**, *313*, 1638.
(37) Bantia, S.; Arnold, C.; Parker, C.; Upshaw, R.; Chand, P. *Antiviral Res.* **2006**, *69*, 39.
(38) Couto, I.; Costa, S. S.; Viveiros, M.; Martins, M.; Amaral, L. *J. Antimicrob. Chemother.* **2008**, *62*, 504.
(39) Thanacoody, H. K. R. *Br. J. Clin. Pharmacol.* **2007**, *64*, 566.
(40) Klemm, A.; Steiner, T.; Flötgen, U.; Cumme, G. A.; Horn, A. *Methods Enzymol.* **1997**, *280*, 171.
(41) Massey, V.; Schopfer, L. M. *J. Biol. Chem.* **1986**, *261*, 1215.
(42) Bourne, C. R.; Bunce, R. A.; Bourne, P. C.; Berlin, K. D.; Barrow, E. W.; Barrow, W. W. *Antimicrob. Agents Chemother.* **2009**, *53*, 3065.
(43) Bennett, B.; Langan, P.; Coates, L.; Mustyakimov, M.; Schoenborn, B.; Howell, E. E.; Dealwis, C. *Proc. Natl. Acad. Sci., U. S. A.* **2006**, *103*, 18493.
(44) Lee, H.; Reyes, V. M.; Kraut, J. *Biochemistry* **1996**, *35*, 7012.
(45) Osborne, M. J.; Schnell, J.; Benkovic, S. J.; Dyson, H. J.; Wright, P. E. *Biochemistry* **2001**, *40*, 9846.

DOI: 10.1021/jacs.5b01442
J. Am. Chem. Soc. 2015, 137, 8983−8990